Earthquakes and Structures, *Vol. 17, No. 3* (*2019*) *245-256*
DOI: https://doi.org/10.12989/eas.2019.17.3.245

Seismic responses of a free-standing two-story steel moment frame equipped with a cast iron-mortar sliding base

Yu-Lin Chung *[1], Kuan-Ting Kuo[1], Takuya Nagae[2] and Koichi Kajiwara[3]

[1]*Department of Architecture, National Cheng Kung University, 701, No.1, University Road, Tainan City, Taiwan*
[2]*Department of Architecture, Nagoya University, Furo-cho, Chikusa-ku, Nagoya, 464-8601, Japan*
[3]*Hyogo Earthquake Engineering Research Center, National Research Institute for Earth Science and Disaster Resilience, 1501-21, Nishikameya, Mitsuda, Shijimi-cho, Miki, Hyogo, 673-0515, Japan*

(*Received March 29, 2019, Revised June 4, 2019, Accepted June 5, 2019*)

Abstract. An experimental study was conducted to evaluate the dynamic behavior of a free-standing frame equipped with a movable base system using cast iron and mortar as the bearing materials. The preliminary friction test indicated that a graphite layer developed on the interface and exhibited stable friction behavior. The friction coefficient ranged from 0.33 to 0.36 when the applied normal compression stress ranged from 2.6 to 5.2 MPa. The effect of the variation of normal compression stress would be small. Shaking table tests on the free-standing frame showed that rock, slide, and rock-slide responses occurred. The cumulative slide distance reached 381 mm under JMA Kobe wave excitation; however, only a few cyclic slides occurred at the same locations along the moving track. Most surfaces sustained single slides. Similar results can be observed in other shaking conditions. The insufficient cyclic sliding and significant rocking resulted in a few graphite layers on the mortar surfaces. Friction coefficients were generally similar to those obtained in the preliminary friction tests; however, the values fluctuated when the rocking became significant. The collisions due to rocking caused strong horizontal acceleration responses and resulted in high friction coefficient. In addition, the strong horizontal acceleration responses caused by the collisions made the free-standing specimen unable to reduce the input horizontal acceleration notably, even when slippage occurred. Compared with the counterpart fixed-base specimen, the specimen equipped with the iron-mortar base could reduce the horizontal acceleration amplification response and the structural deformation, whereas the vertical acceleration response was doubled due to collisions from rocking.

Keywords: friction coefficient; slide; movable base; mortar; cast iron; steel frame; shaking table test

1. Introduction

In earthquake events, middle-to-low rise buildings tend to sustain the most damage. In the 1999 Chi-Chi earthquake, approximately 92% of the damaged buildings were those with fewer than six stories, and 50% of the damaged low-rise buildings were classified as being severely damaged (Hsiao *et al*. 1999). In the 1995 Kobe earthquake, approximately 86% of the damaged steel structures had fewer than six stories (AIJ 1997). Similar results can be observed for reinforced concrete structures. Most of the damaged buildings are residential buildings and houses. The first stories of such buildings sustained the most severe structural damage. Column base failure reduces story resistance and might lead to a collapse mechanism even if plastic behaviors are developed in the beam-column connections. Numerous steel column base failures occurred as a result of the 1995 Kobe earthquake and caused severe damage (AIJ 1997). Structural irregularities due to the spatial requirements of businesses, car parking spaces, or the architectural demands of open spaces might cause a soft-story or weak-story in the bottom story. Such failures are one of the major causes of severe damage, including collapses from the 1999 Chi-Chi earthquake, which spread from reinforced concrete residential buildings and reinforced-brick street houses (Hsiao *et al*. 1999, Tsai *et al*. 2000). To enhance the seismic capacity of buildings, isolating the seismic forces applied to buildings by applying a movable base, including foundation or column bases, to the structure is considered an effective strategy. Rubber bearings are common isolators for elongating the natural period of the structure due to the low stiffness of the bearings, and the response can be reduced by applying additional damping (Bakhshi *et al*. 1998, Chang *et al*. 2002, Tiong *et al*. 2014, and Mostaghel *et al*. 1987). Sliding-type bearings, such as friction pendulum systems, for use as core elements of base-isolated structures, have been developed to minimize the friction coefficients of sliding interfaces (Constantinou *et al*. 2007, Fakhouri *et al*. 2013, Mokha *et al*. 1990, 1991, Tsopelas *et al*. 1996, Zayas *et al*. 1990, Amiri *et al*. 2017). Due to their high cost and maintenance demands, base-isolated systems are mostly applied to critical facilities such as hospitals and other public infrastructure. For low-cost apartments or houses, a movable base system may be more cost efficient.

A movable base system had been proposed using common construction materials on the base-supporting

*Corresponding author, Assistant Professor
E-mail: ylchung@mail.ncku.edu.tw

Copyright © 2019 Techno-Press, Ltd.
http://www.techno-press.com/journals/eas&subpage=7
ISSN: 2092-7614 (Print), 2092-7622 (Online)

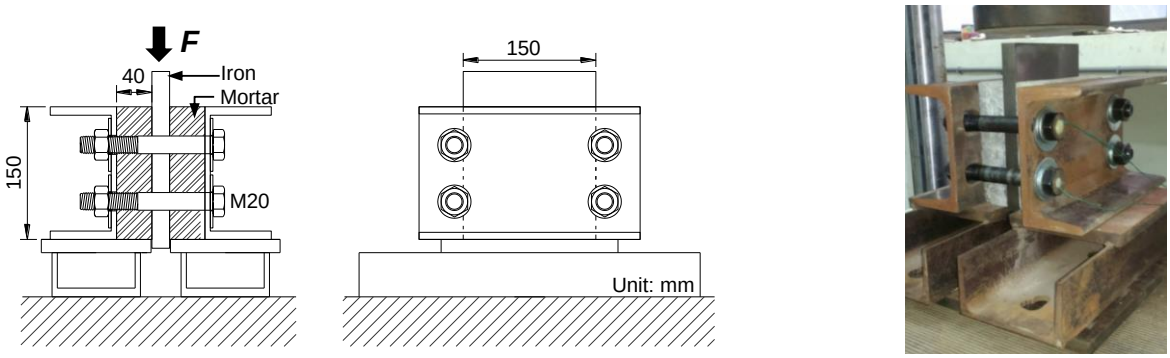

(a) (b)

Fig. 1 Test setup: (a) design of the test and specimen; (b) overall view of the setup

interface to develop a simple sliding mechanism. A stable and appropriated friction coefficient could prevent the building from being subjected to severe damage or even collapsing so that repair costs can be minimized. Furthermore, this can prevent the building from sliding under minor shaking and can minimize the possibility of water, gas, or electricity failure, which frequently occur in high-seismic-risk areas. Friction tests on various materials have been conducted, revealing friction coefficients of approximately 0.8 for steel to steel (Campbell *et al*. 1939), 0.4–0.5 for mortar to mortar (Tassios *et al*. 1986), and 0.6–0.8 for steel to mortar (McCormick *et al*. 2009, Rabbat *et al*. 1985). The values are too high to result in a reduction in damage. Enokida conducted shaking table tests on a free-standing structure equipped with various materials for slide interfaces (Enokida *et al*. 2018). The specimens were designed to have a low center of gravity to prevent rock response. The results indicated that the maximum coefficients of steel to mortar, ductile iron to mortar, Gray iron to mortar, and an interface with a graphite layer were 0.82, 0.28, 0.3, and 0.22, respectively. The kinematic friction coefficients of the ductile iron–mortar, gray iron–mortar, and graphite layer interfaces were found to have an almost constant value of 0.2 during sliding. Iron is a ferroalloy containing 1.8-4.0% of graphite. The graphite layer developed under sliding was found to be effective to reduce the friction coefficient in the interfaces of iron and mortar. In 2015, full-scale shaking table tests were conducted in E-Defense to evaluate the seismic performance of a free-standing 10-story reinforced concrete (RC) building using a gray iron–mortar movable base (Kajiwara *et al*. 2017, Sato *et al*. 2017, Tosaichi *et al*. 2017). The measured friction coefficient between iron and mortar was approximately 0.2. The maximum drift angle was only 0.6% under 100% JMA Kobe wave intensity shaking. The maximum drift angle reached 3% of that of the counterpart, namely the fixed-base specimen. The reduction in the maximum deformation was notable. Rocking, sliding, and rocking-sliding responses were observed and the friction coefficient varied significantly under intensive shaking. Base uplift induced by the rock behavior of the structure can cause variations of compression stress, stress concentration and impact on the mortar surface. The effects of this on the friction coefficient and structural responses such as the floor acceleration response are still unclear. In a real case, it is unlikely that the sliding interface will be cleaned or repaired, and the building will be recentered immediately after the mainshock of an earthquake event. The slide behavior with respect to the surface condition under the continuous loading of the intensive aftershock requires further examination.

An experiment was employed in the study to investigate the seismic behavior and performance of a free-standing building equipped with a movable iron-mortar base. The preliminary friction tests on the iron–mortar materials have been conducted by applying various normal compressions to evaluate the effect of this on the friction coefficient. A full-scale, two-story steel moment frame equipped with an iron-mortar base was prepared and tested by using shaking table facilities. Two seismic records with different characteristics were continuously input with increasing intensity to observe the dynamic behaviors including sliding, rocking and rocking-sliding and to understand effects on the friction behavior. The structural responses in terms of acceleration responses and deformations were examined and compared with that of a fixed-base specimen to evaluate its performance under critical loading scenarios.

2. Friction behavior of the iron-mortar interface

2.1 Preliminary friction tests

Normal compression on an iron-mortar movable base varies under shaking. Tests have indicated that the friction coefficient might change under different normal compression conditions (Enokida *et al*. 2018, Kajiwara *et al*. 2017, Sato *et al*. 2017, Tosaichi *et al*. 2017). To examine the effect of such conditions, a friction test on two materials was conducted. Gray iron, the most common type of cast iron, has a strength of 150–350 N/mm^2. The tested FC250 cast iron has a carbon constituency of 3.01%. The series number corresponds to tensile strength. The mortar specimen has a measured strength of 350 kg/cm^2, water cement ratio of 0.41, and fineness modulus of 2.7. The test setup is shown in Fig. 1. The FC250 plate with the dimension of 200 mm×150 mm×20 mm was sandwiched between two mortar blocks that were both 150 mm×150 mm×40 mm. The test unit was clipped by two channels using four M20 bolts to fasten it from the outside of the

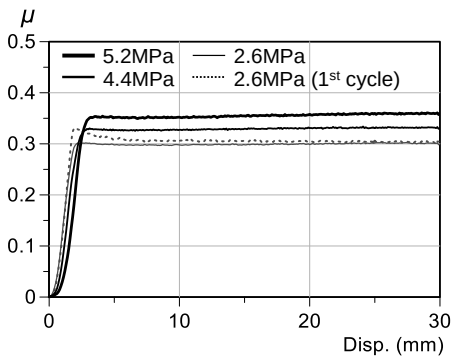

Fig. 2 Friction coefficient under various compression stress conditions

specimen. Monotonic push was applied for a 30 mm amplitude, and then the setup was revised to a 180° angle to load the specimen again. The monotonic tests were repeated for eight cycles. The normal compression stress values applied on the surfaces were 2.6, 4.4, and 5.2 MPa, which were similar with values of 2.2 to 4.5 MPa adopted in the 10-story R.C. building test (Kajiwara *et al*. 2017), and were controlled by the pretension forces of bolts under the bolt monitoring gauges. The load speed was at a constant rate of 30 mm/min.

2.2 Test results

Fig. 2 presents the friction coefficients (μ) under various normal compression stress conditions. The coefficients are obtained by dividing the load cell readings by the compression forces measured from the bolt gauges. A slightly higher friction coefficient appeared in the initial cycle and was then reduced to a constant value while the interface was sliding, as indicated by the dotted line in Fig. 2. From around the second cycle, the peak disappeared, resulting in a bilinear response behavior. Similar results can be observed in the study of Enokida (2018); the maximum friction coefficient disappeared after a few cycles and become a constant value of the kinetic friction coefficient. The solid lines in Fig. 2 represent the averaged values of the rest of the cycles. The averaged coefficients were 0.3, 0.33, and 0.36 under the normal compression stress values of 2.6, 4.4, and 5.2 MPa, respectively. The coefficient increased slightly with an increase in normal compression stress. The effect of the variation of normal compression stress would be small.

The sliding surface of the mortar is presented in Fig. 3(a). The surfaces did not make complete contact, even though the mold was fabricated and assembled to be as flat as possible. The surface shows the original condition and the contacted area covered by the graphite layer. The boundary of the contact surface was amplified to 10 times its original size using a microscope [Fig. 3(b)]. The boundary of the graphite layer was covered with graphite powder. Fig. 3(c) presents an amplified image of the contact surface. Scratch could be identified and graphite powder was separated in the deep holes.

Fig. 4(a) shows the surface of the iron plate. The surfaces of the plate were milled using a CNC machine after the plate had been removed from the mold. Fig. 4(b) presents the surface of the uncontacted area. The diagonal scotches made by the CNC machining can be observed. When the plate was rubbed with mortar for cycling, most of the shallow diagonal scratches were erased and a graphite

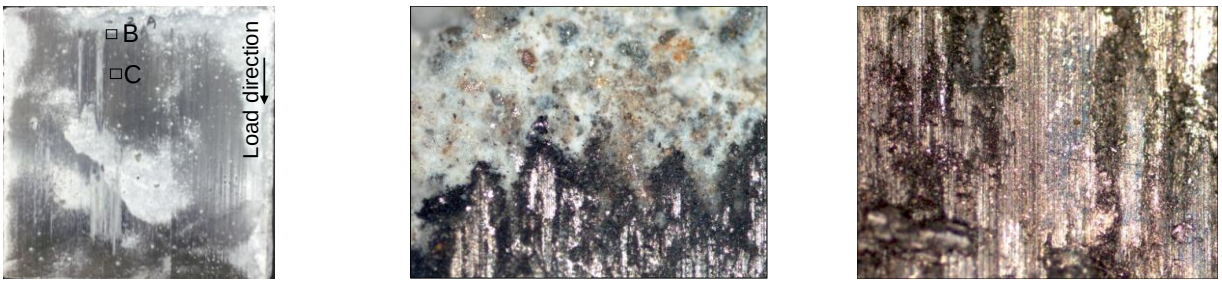

(a) (b) (c)

Fig. 3 Mortar surface observation: (a) surface of the mortar; (b) 10× magnification of Location B; (c) 10× magnification of Location C

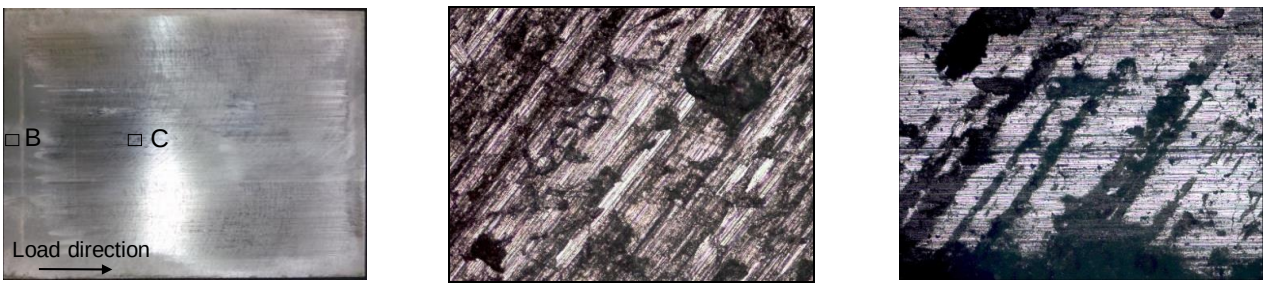

(a) (b) (c)

Fig. 4. Iron surface observation: (a) surface of the iron; (b) 10× magnification of Location B; (c) 10× magnification of Location C

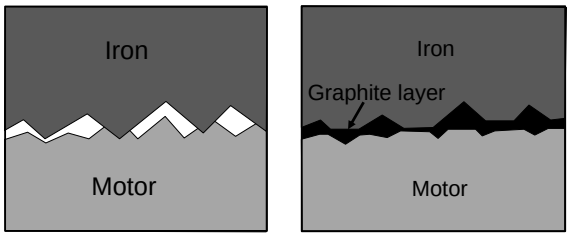

(a) (b)

Fig. 5 Condition of the sliding interface: (a) initial condition; (b) condition after a few cycles

layer developed on the surface. The deep diagonal scratches remained and contained black graphite powder, as shown in Fig. 4(c).

Based on the aforementioned observations (see Figs. 2–4), the initial roughness of the surface might be the reason behind the initial high friction coefficient. When the shallow surface roughness was eliminated and the graphite layer developed on the interface, the maximum friction coefficient become nonsignificant and close to the constant kinetic friction coefficient. The lubrication states are illustrated in Fig. 5.

3. Shaking table tests on the full-scale free-standing frame

Tests were conducted using the new shaking table facility in the south laboratory of the National Center of Research on Earthquake Engineering (NCREE), Taiwan. The three-directional table features plane dimensions of 8 m×8 m. Specimens with a maximum weight of 2500 kN can be accommodated on the table, which is operated by eight servo-hydraulic actuators. The reaction forces of the actuators are provided by a 35-MN weight reaction mass isolated from the fixed foundation by 120 air springs and 192 viscous dampers, as shown in Fig. 6. The maximum horizontal stroke and velocity reach ±1 m and ±2 m/s, respectively. The maximum horizontal and vertical accelerations for the bare table are ±2.5 g and ±3 g, respectively. Its high performance means the table can be used to conduct high-speed long-stroke dynamic tests to simulate near-fault pulse-like earthquake waves.

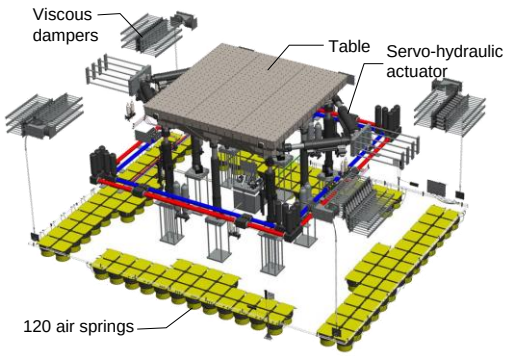

Fig. 6 High-performance shaking table (NCREE)

3.1 Specimen design and test program

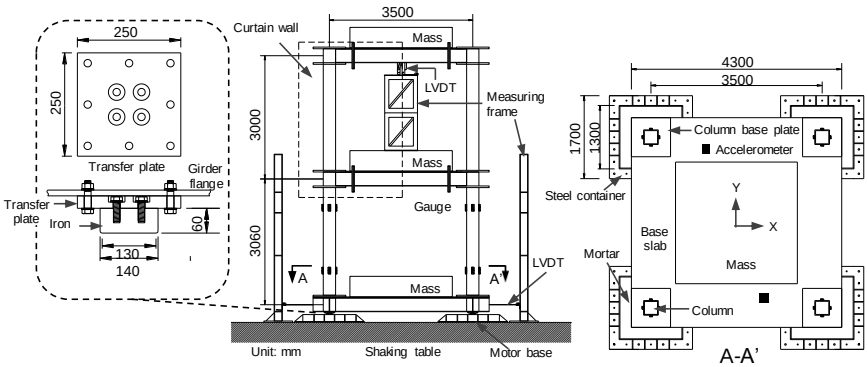

(a)

(b)

(c)

Fig. 7 Specimen design: (a) Two-story test frame and measurements; (b) Free-standing specimen; (c) Fixed-base specimen

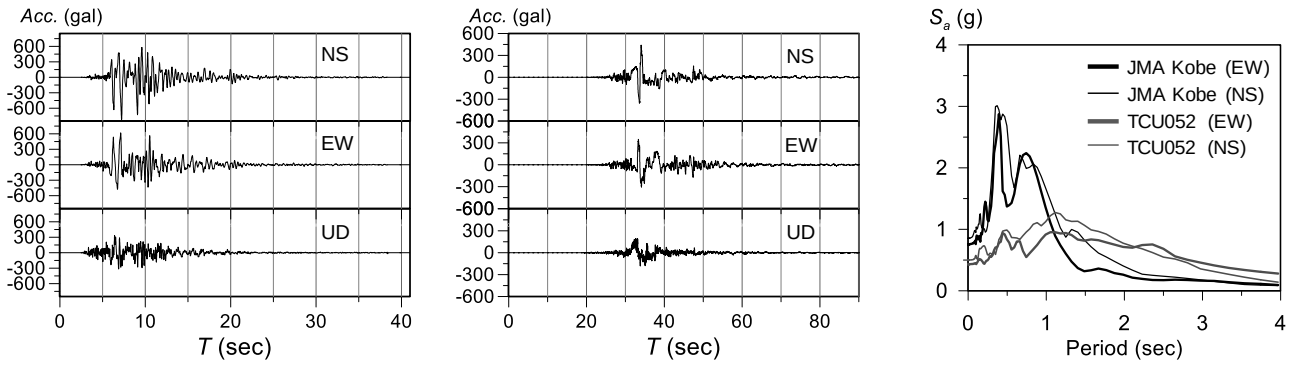

(a) (b) (c)

Fig. 8 Input waves: (a) time history of JMA Kobe; (b) time history of TCU052; (c) response spectra

Table 1 Specification of specimen

Member	Specification	Material
Column	Box 300×9	STKR400
Girder	H340×250×9×14	SN400B
Mass	5 (t)	RC
1st floor weight	11.17	-
2nd floor weight	12.16	-
Roof floor weight	11.17	-
Total weight	34.5	-

Table 2 Test program

Input	Intensity	Specimen
JMA Kobe	25%	Free- standing
TCU052	50%	
JMA Kobe	50%	
TCU 052	100%	
JMA Kobe	100%	
TCU 052	50%	Fixed-base
JMA Kobe	50%	
TCU 052	100%	
JMA Kobe	100%	

An existing two-story, one-span, and one-bay steel moment-resisting frame, which was designed as a test frame for multiple purposes, including the performance evaluation of dampers and nonstructural components, was used for the shaking table tests. The specimen has a 3.5-m span in two plane directions, and the height of each story is approximately 3 m. The members were designed to be robust with the intention that they would be reused. The yield base shear coefficient was approximately 0.5. The specimen was equipped with two different base conditions: a free-standing specimen and a specimen with fixed column bases. As presented in Fig. 7(a), a base slab, which consisted of girders and beams and was topped with a 21-mm-thick steel plate, was bolted to the column bases. This resulted in the height of the first story becoming 3.06 m. An FC250 iron bearing block with dimensions of 140 mm×140 mm×60 mm was bolted to the bottom flanges of the foundational girders at each column location by applying a transfer plate. The four bottom boundaries of the blocks were grinded to round edges, resulting in an effective bearing area of the surface of 130 mm × 130 mm. The specimen was placed on four mortar bases that were mounted on the table. The mortar, which had the same properties as the mortar blocks in the preliminary friction test, was grouted into the steel container with a rebar mesh (rebar diameter: 9.5 mm, spacing: 100 mm). A 5-ton reinforced concrete mass was mounted on each story, making the weight of the specimen 34.5 ton. The compression stress on the iron bearing surface was approximately 5.2 MPa, which is the same as one of the compression conditions in the preliminary friction test. The friction coefficient was approximately 0.36 and the width-to-height ratio of the free-standing specimen was 0.55. The specifications of the members are listed in Table 1. Fig. 7(b) and (c) show overall views of the free-standing and fixed-base specimens, respectively. The column bases of the fixed-base specimen were bolted to the table directly.

Curtain walls were installed on one corner of the second story to evaluate seismic performance. Three-directional accelerometers were installed on two opposite corners of the slab of each story. Displacement transducers were fixed on each floor to obtain the interstory drift, as shown in Fig. 7(a). In addition, a visual movement measurement system was applied to capture the three-dimensional movement of the specimen while it was subjected to shaking.

The ground motion observed at JMA's Kobe Marine Meteorological Observatory during the Southern Hyogo Prefecture Earthquake (hereinafter referred to as JMA Kobe) was used for the excitation wave. The maximum acceleration of the seismic motion was 8.18 m/s^2 in the north-south (NS) direction, 6.17 m/s^2 in the east-west (EW) direction, and 3.32 m/s^2 in the up-down (UD) direction, as shown in Fig. 8(a). One near-fault ground motion recorded in the 1999 Chi-Chi earthquake was also adopted. The ground motion was recorded at the TCU052 station located within 40 km of the epicenter, as shown in Fig. 8(b). The maximum acceleration of the seismic motion was 4.38 m/s^2, 3.47 m/s^2, and 1.94 m/s^2 for the NS, EW and UD directions, respectively.

The intensity was approximately 50% of the JMA Kobe wave. Both of the two ground motions showed higher intensity in the NS direction. The NS and EW components were input in the *Y* and *X* directions of the table (Fig. 7(b) and (c)). The pseudo acceleration response spectra of the

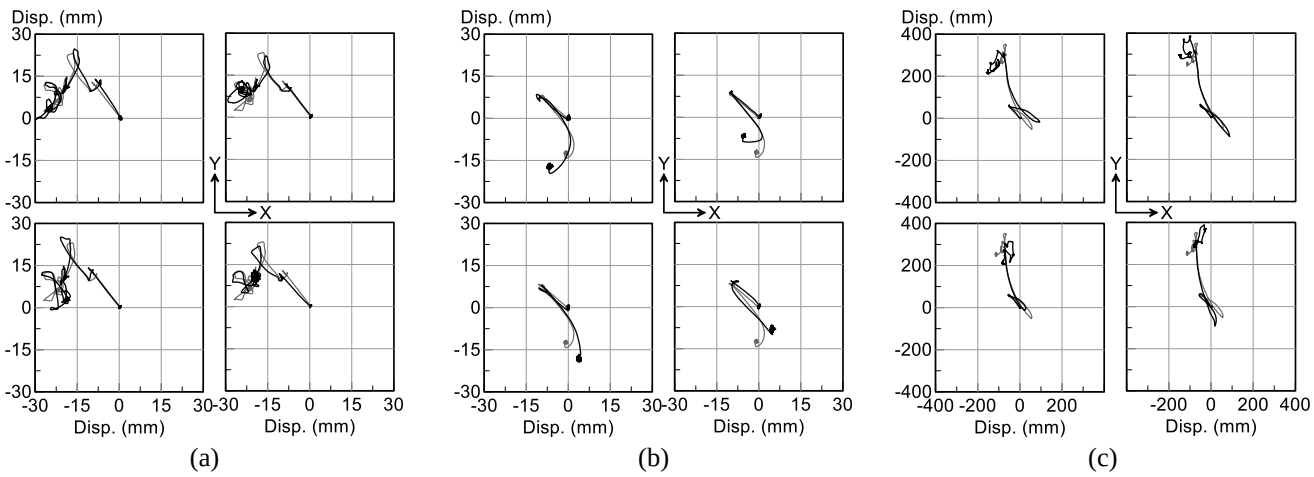

Fig. 9 Movement of the specimen: (a) JMA Kobe 50%; (b) TCU052 100%; (c) JMA Kobe 100%

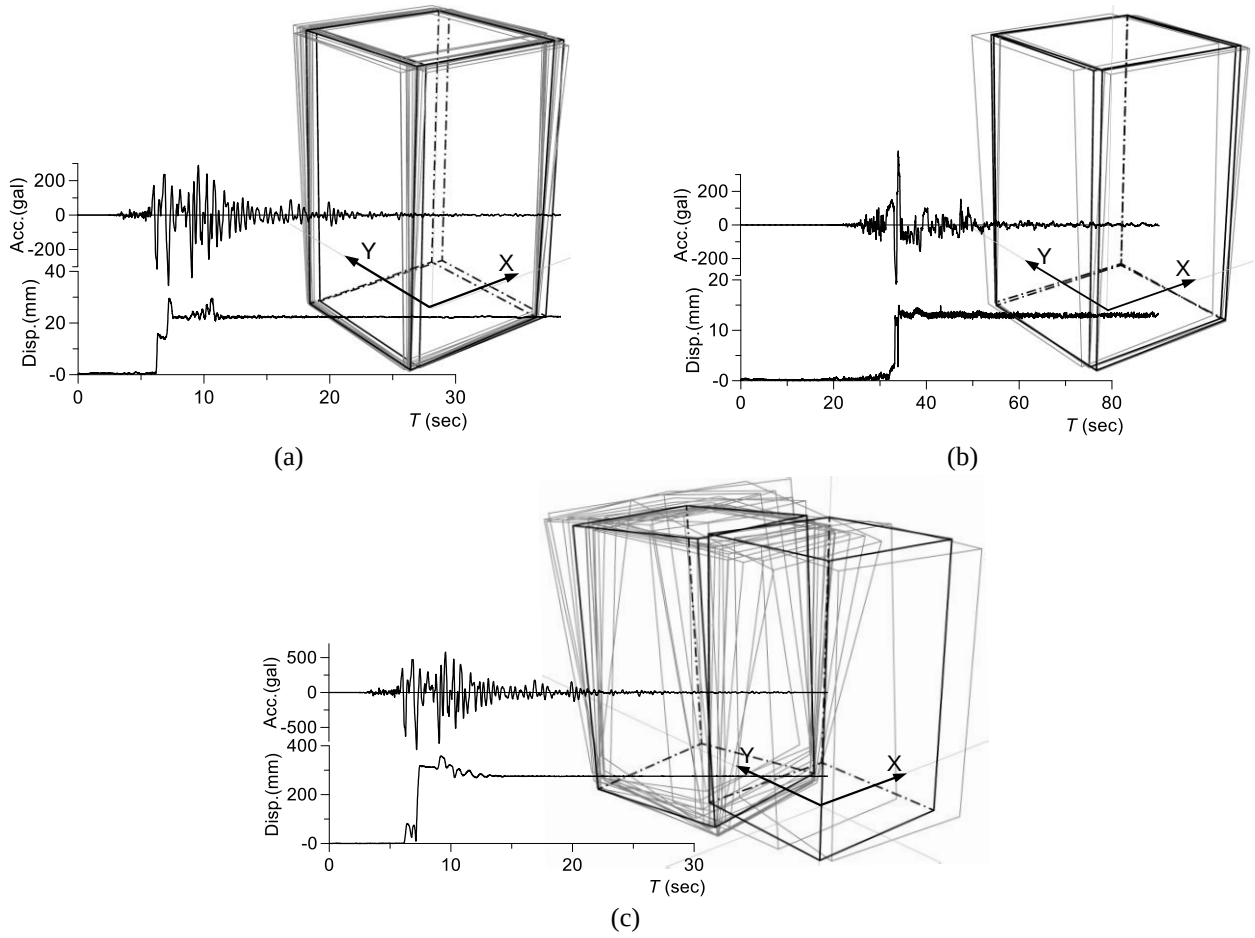

Fig. 10 Three-dimensional movement of the specimen while subjected to (a) JMA Kobe 50%; (b) TCU052 100%; and (c) JMA Kobe 100% waves

ground motions are presented in Fig. 8(c). The JMA Kobe wave exhibited a strong response at approximately 0.36 s and 0.75 s, whereas the predominant period of the TCU052 was at approximately 1.1 s. The excitation tests were performed in the program sequence shown in Table 2, with gradually increasing amplitude of vibration for both test cases, that is, the free-standing test and the fixed-base test. White-noise inputs with an RMS of 0.6 m/s^2, duration of 70 s, and frequency bandwidth of 0.1–50 Hz were applied prior to each main test. The first model periods of the free-standing and fixed-base specimens were 0.31 and 0.29 s, respectively.

3.2 Test results

3.2.1 Sliding and rocking behaviors

Sliding was observed in the JMA Kobe 50%, TCU052 100%, and JMA Kobe 100% shakings. Fig. 9 presents the

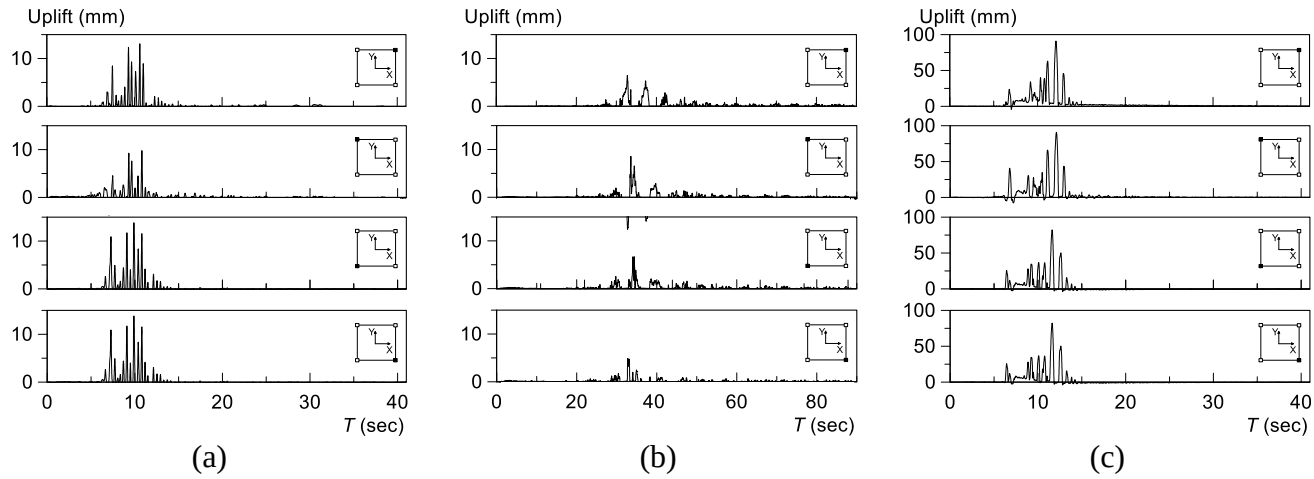

Fig. 11 Uplift response time history: (a) JMA Kobe 50%; (b) TCU052 100%; (c) JMA Kobe 100%

horizontal moving tracks of the four iron bearing blocks under shaking conditions. The locations of the four foundations are illustrated in Fig. 7. The gray line represents the movement of the mass center of the base slab obtained by averaging the displacements of the four bearing blocks. The JMA Kobe 50% excitation induced the maximum displacement of approximately 30 mm, and the specimen eventually stopped at a location approximately 20 mm to the left of the original position. The track of the mass center followed those of the four iron bearing blocks, which indicates that the translation movement dominated the response (Fig. 9(a)). For the TCU052 100% shaking, the track line became less complex compared with that of the JMA Kobe 50% shaking. One cycle of the oblique movement can be observed. The maximum and residual displacements were both approximately 15 mm. The tracks of the four iron bearing blocks showed slight differences to the mass center at the end of the movement. Small planar torsion was confirmed by visual observations conducted after the shaking. When the input intensity of the JMA Kobe wave reached 100%, the maximum displacement was increased substantially to approximately 400 mm. According to the tracks shown in Fig. 9(a)-(c), few of the moving tracks overlapped under the three seismic loadings. Because the specimen was not moved back to its original position after each shaking experiment, the friction interfaces on the moving tracks mostly experienced single slide, without multiple cycles of sliding. The graphite layers might not be sufficiently developed and the initial surface roughness might have made the friction coefficient vary under the shakings as observed in preliminary friction tests.

The three-dimensional movements of the free-standing specimen obtained using the visual movement measurement system are illustrated in Fig. 10. The NS component of the input time history, and the root sum square of the vertical displacement and two horizontal displacements of the mass center of the base slab are also presented in each figure. Black outlines represent the initial and final specimen positions. Gray outlines represent the instant movement of the specimen under the peak responses. The JMA Kobe 50% excitation induced substantial slides during the first two intensive shakes. After reaching a maximum displacement of 30 mm, the specimen slightly slid back to 20 mm and kept rocking during the last part of the input time history (Fig. 10(a)). The rocking responses caused short displacements around the final position, as shown in Fig. 9(a). For the TCU052 100% shaking shown in Fig. 10(b), the specimen slid upon the strongest shake and caused a cycle of sliding, as shown in Fig. 9(b). Rocking responses became gentler than that of the JMA Kobe 50% shaking. When the input intensity of the JMA Kobe wave reached 100%, the intensive shakes induced significant rocking and sliding responses (Fig. 10(c)). The intensive NS component of the ground motion caused a strong response in the Y direction. The rocking started upon the first strong shake and the horizontal movement occurred immediately before the uplifted iron bearing blocks made contact with the mortar. The horizontal movement caused a residual displacement of approximately 300 mm. Then, multiple cycles of rock and rock-slide behaviors occurred in the later part of the input time history and slightly reduced the residual displacement to approximately 250 mm. The rock and rock-slide behaviors notably increased under this shaking condition. The intensive acceleration input tended to cause the uplifted mass center of the specimen to slide at the same time. Comparing the initial and final positions of the specimen revealed that planar torsion occurred. The center of rigidity of friction resistance against the base slide moved away from the specimen's center of gravity due to uplift, which may explain why the base slide was accompanied by a rotational movement.

The uplift response of each iron bearing block is presented in Fig. 11. The uplifts became stronger in the second half of the JMA Kobe 50% shaking experiment (Fig. 11(a)). The maximum uplift reached 14 mm. The uplift was gentle under TCU052 100% shaking (Fig. 11(b)). As revealed in the sliding behavior shown in Fig. 9(b) and Fig. 10(b), sliding dominated the responses. The longer-period components of the waves might have been responsible for this. The maximum uplift was approximately 6 mm. For the JMA Kobe 100% excitation, the maximum uplift also occurred during the second half of the shaking experiment and the uplift value reached 91 mm, which was amplified to 6.5 times that of the 50% intensity (Fig. 11(c)). As shown in

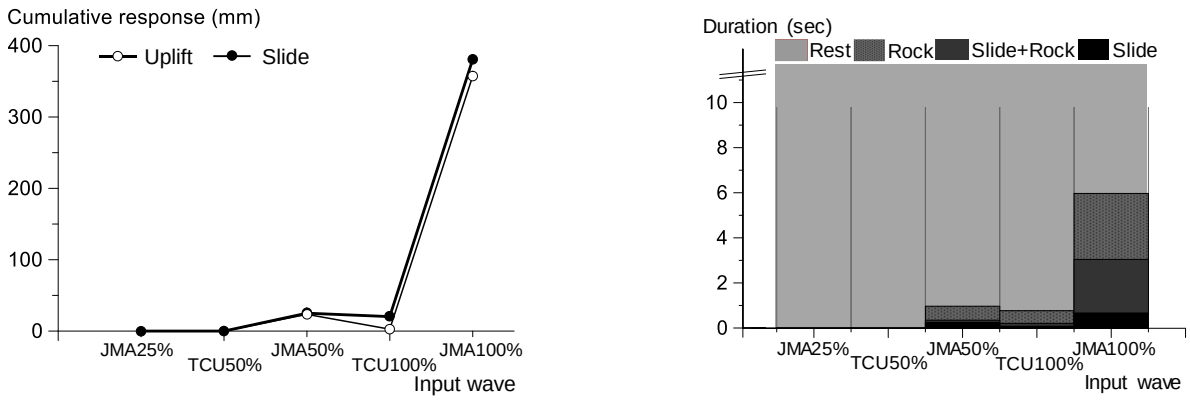

(a) (b)

Fig. 12 Sliding and rocking responses: (a) cumulative uplifts and slides of columns; (b) contribution of each response modes

(a) (b)

(c)

Fig. 13 Observation of the motor base surfaces: (a) after JMA Kobe 50% shaking; (b) after TCU052 100% shaking; (c) after JMA Kobe 100% shaking

Fig. 10(c), the rocking response accompanied sliding and moved the specimen back slightly toward the original position.

Fig. 12 summarizes the cumulative movements of the specimen. The cumulative uplifts and cumulative slide displacements of the mass center of the base slab under each shaking condition are presented in Fig. 12(a). Slide displacement is defined as the horizontal displacement of a specimen. During this time, the instant uplifts of the iron blocks were all smaller than 3 mm. The cumulative uplifts in the JMA Kobe 50%, TCU052 100%, and JMA Kobe 100% shakings were approximately 25, 4, and 357 mm, respectively. Furthermore, the cumulative sliding distances were 25, 20, and 381 mm, respectively, under the three aforementioned shaking conditions. The cumulative uplift and slide both significantly increased by approximately 15 times when the intensity of the JMA Kobe wave was enhanced from 50% to 100%.

Cumulative movement durations of the responses, namely rock, slide, and rock-slide, were calculated based on the response time histories (Fig. 12(b)). Based on the horizontal displacement and uplift time history of the mass center of the base slab, rock-slide behavior was defined as uplift and horizontal movement of the specimen occurring simultaneously. The rock-slide behavior became notable under the JMA 100% excitation. The cumulative durations of the rock and rock-slide responses increased to 2.9 and 2.4 s, respectively. The total duration of rock and rock-slide behaviors was 5.5 s, which was approximately 8.9 times the rock duration observed in the JMA Kobe 50% excitation. The slide duration increased to from 0.26 s to 0.68 s. The notably increased uplift amplitudes and uplift cycles lead to a longer duration of rock-related movements.

The surface conditions of the mortar bases are shown in Fig. 13. The JMA Kobe 50% shaking developed few graphite layers on the surface (Fig. 13(a)). Similar conditions could be observed after TCU052 100% shaking (Fig. 13(b)). The JMA Kobe 100% shaking exhibited considerably strong slide, rock, and rock-slide responses. Large residual displacement can be observed in Fig. 13(c). The intensive impact during rocking caused surface crushes in several locations. Graphite layers were developed in

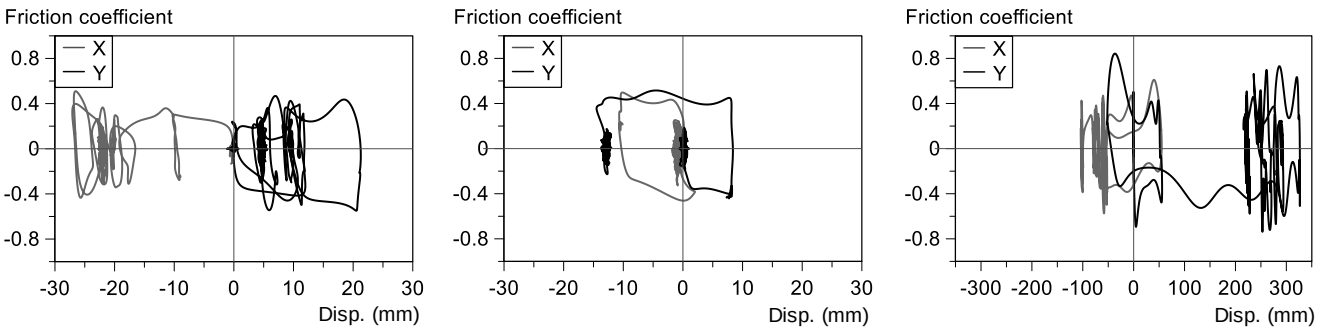

(a) (b) (c)

Fig. 14 Friction coefficient: (a) JMA Kobe 50%; (b) TCU052 100%; (c) JMA Kobe 100%

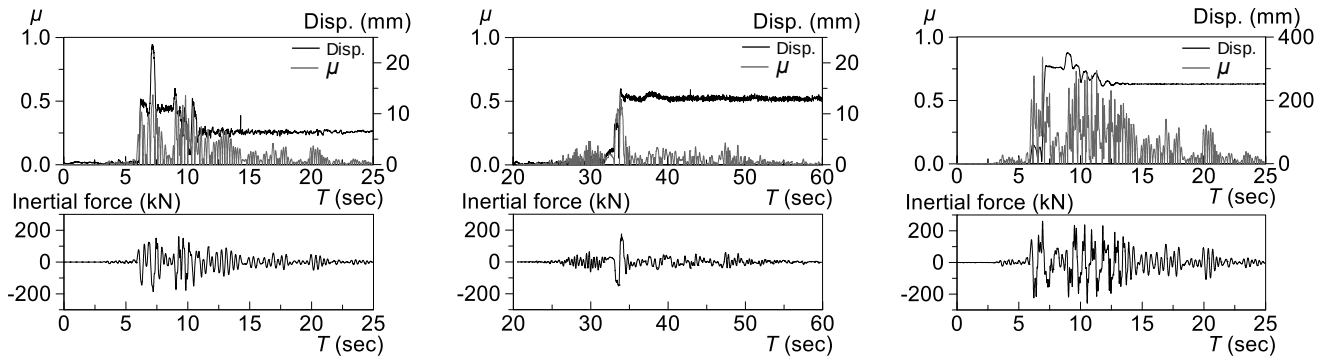

(a) (b) (c)

Fig. 15 Friction coefficient, displacement response, and base shear force time-history while subjected to (a) JMA Kobe 50%; (b) TCU052 100%; and (c) JMA Kobe 100% excitations

several locations on the tracks. Friction coefficient and friction behavior might be effected by the insufficient graphite layer and unsmooth surface.

3.2.2 Friction coefficient

Fig. 14(a)–(c) presents the friction coefficient and slide amount of the mass center of the base slab in both base slide directions while it was subjected to JMA Kobe 50%, TCU052 100%, and JMA Kobe 100% shakings. The friction coefficient while the base was sliding was estimated from the horizontal inertial force, which is obtained by obtaining the sum of the story weights and multiplying it by the acceleration generated at each story, and the weight, which considers the effect of vertical input acceleration. The equation is as follows.

$$\mu=\left(\sum_{Base}^{R} m_i \cdot \alpha_{Hi}\right)/(M \cdot g - M \cdot \alpha_Z) \tag{1}$$

where m_i is the mass at each story, α_{Hi} is the horizontal acceleration at each story, M is the total mass of the specimen, g is the gravitational acceleration, and α_Z is the vertical acceleration at the shaking table. The friction coefficient under JMA Kobe 50% shaking show larger variations than that of the TCU052 100% shaking condition. The coefficient of static friction was in the range of 0.4 to 0.43 at the start of base slippage, and the coefficient of kinetic friction was approximately in the range of 0.35 to 0.4 while the base was slipping (Fig. 14(a)). The coefficients of static friction and kinetic friction while subjected to the TCU052 100% excitation were approximately 0.43 and 0.37, respectively (Fig. 14(b)). The values generally agreed with the preliminary friction test results, whose friction coefficients were 0.36 under compression of 5.2 MPa. For the JMA Kobe 100% excitation, as shown in Fig. 14(c), the friction coefficient fluctuated. The maximum static friction coefficient notably increased and reached 0.8, and the kinetic friction coefficient was approximately 0.35.

Fig. 15 presents the absolute value of the friction coefficient time history together with the displacement time history, which was the root sum square of the horizontal displacement and the vertical displacement of the mass center of the base slab. The horizontal inertial force time history, which is the numerator of Eq. (1), is also illustrated. Due to the larger intensity of the NS component of the input waves, responses in the Y direction were only considered in the figures. According to the upper parts of Fig. 15(a) to (c), the rocking responses tended to be rhythmical with high friction coefficients, especially under the JMA Kobe 100% excitation. In addition, from the bottom portions of Fig. 15 (a) and (c), the horizontal inertial force in JMA Kobe 100% shaking were approximately twice that of the JMA Kobe 50% shaking, while the vertical acceleration input had a relatively small effect compared with gravity. The acceleration response of the free-standing frame appears to have been amplified by an increasing intensity of the inputs, especially under the collisions caused by the rocking response, leading to a large friction coefficient and

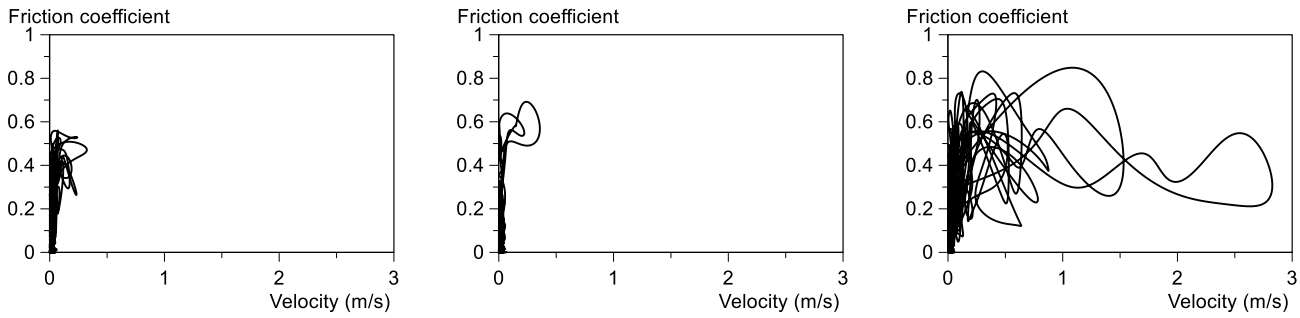

Fig. 16 Friction coefficient versus velocity relationships under (a) JMA Kobe 50%; (b) TCU052 100%; and (c) JMA Kobe 100% waves shakings

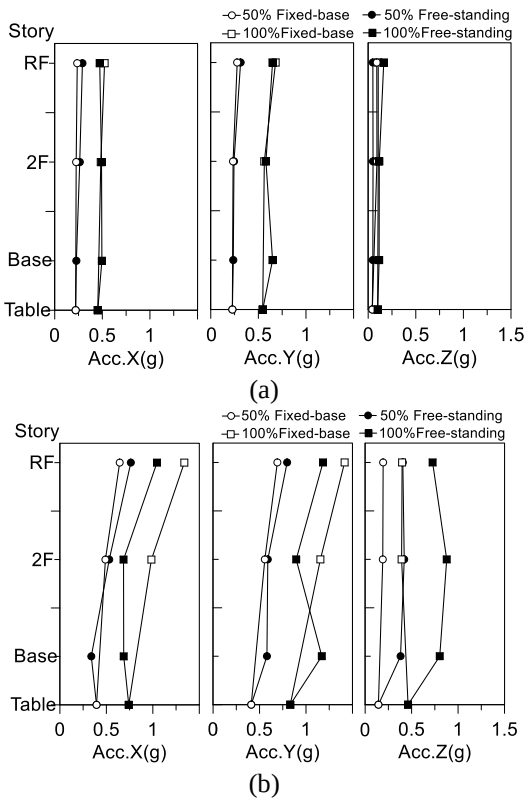

Fig. 17 Floor acceleration responses: (a) response under TCU052; (b) response under JMA Kobe

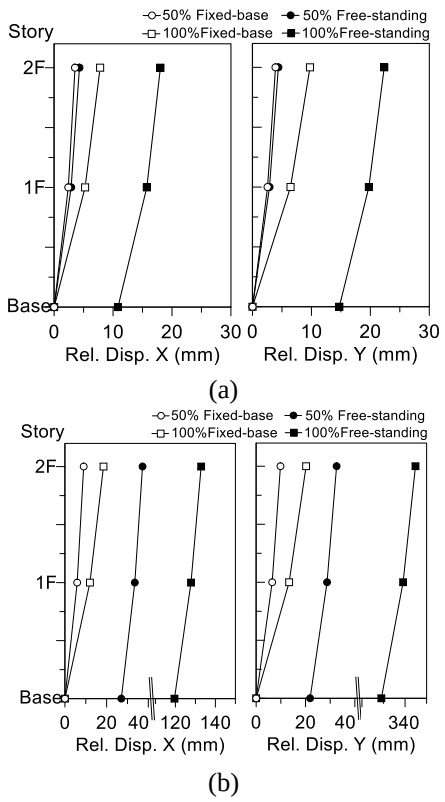

Fig. 17 Floor acceleration responses: (a) response under TCU052; (b) response under JMA Kobe

variation. The acceleration distribution of the frame is discussed in the following passages.

The friction coefficients calculated from the combination of the two horizontal components, and base slide velocity relationships are presented in Fig. 16. The base slide velocity is presented as the relative velocity of the base slab with respect to the shaking table velocity. Each velocity value was obtained by integrating the measured acceleration by the average acceleration method. Responses in the JMA Kobe 50% and TCU052 100% shakings were not notable due to the low velocity. In the JMA Kobe 100% shaking condition (Fig. 16(c)), the friction coefficient varied from 0.3 to 0.8 in the lower velocity range and the coefficient tended to converge to a constant value of approximately 0.35 when the velocity exceeded 1.5 m/s. Similar response can be observed in previous 10-story RC frame tests (Tosaichi *et al*. 2017). From the test results of Enokida (2018), whose specimen had a very low center of gravity and rocking did not occur under the shaking condition, the friction coefficient was constant under different velocity levels. This finding, combined with the observations of the friction coefficient time history and the displacement time history relationship (Fig. 15(c)), indicates that the rock response, which exhibited smaller horizontal velocity than that of slide response, may be responsible for the large variations in the friction coefficients.

3.2.3 Structural responses

Fig. 17 summarizes the maximum floor acceleration response along the height of the free-standing and fixed-base specimens while they are subjected to various loading

conditions. Under the TCU052 wave excitations, responses in the structures were almost unamplified compared with the inputs, as presented in Fig. 17(a). The two specimens showed similar responses in the horizontal and vertical directions, although slippage occurred in the free-standing specimen. This might be because the input acceleration ratio was close to the friction coefficient. Horizontal responses under the excitations of JMA Kobe waves were both amplified, especially in the fixed-base specimen (Fig. 17(b)). The horizontal responses of the free-standing specimen were generally similar and slightly larger than that of the fixed- base specimen under the 50% intensity shaking. When the input intensity was increased to 100%, the horizontal responses of the free-standing specimen were not reduced compared with the input, except the base and second story responses in the *X* direction of the free-standing specimen. Compared with the fixed-base specimen, horizontal responses of the free-standing specimen were substantially smaller. The roof acceleration in the *X* direction was reduced from approximately 1.4 g to 1.2 g. The response was reduced by approximately 20%. Similar responses can be observed in the *Y* direction. Substantial sliding might be responsible for the reduction. The base response in the *Y* direction was amplified to 1.4 g, which might have been caused by the substantial rocking that occurred in the direction. Vertical responses in the free-standing specimen were amplified approximately 2-fold, with the collision due to rocking responsible for this.

Responses in terms of the maximum inter-story relative displacements are presented in Fig. 18. The response at the base represents the relative displacement between the base slab and the shaking table. For the TCU052 wave excitations, the responses were similar in the 50% intensity shaking. For the 100% loading, the maximum relative interstory displacements of the structure were reduced slightly due to the base sliding, as shown in Fig. 18(a). For the JMA Kobe 50% shaking, which had a similar intensity to the TCU052 100% shaking, the maximum relative interstory displacements of the first story of the free-standing specimen were approximately 6.5 and 6.9 mm in both directions, with drift angles of approximately 0.24% and 0.26%, respectively. The values were similar to those for the fixed-base specimen. When the input intensity was increased to 100%, the maximum relative interstory displacements in the two directions of the first story of the fixed-base specimen were 12 and 13.4 mm, with relative drift angles of 0.44% and 0.5% in the two directions. The drift angles in the free-standing specimen were 0.31% and 0.37%. The maximum deformation was reduced by approximately 30% in the frame with the movable base system.

5. Conclusions

A series of shaking table tests on a full-scale, two-story, one-span, one-bay, steel moment frame equipped with a mortar-iron slide base were conducted to evaluate the seismic responses. A counterpart test with the fixed-base specimen was also conducted to compare the responses of the structures. The major observations were as follows.

- The preliminary friction test on the iron-mortar surface showed that graphite layer was developed on the interface and exhibited a stable and constant friction coefficient. The averaged kinetic friction coefficients were 0.3, 0.33, and 0.36 under the normal compression stress of 2.6, 4.4, and 5.2 MPa, respectively. The coefficient slightly increased with an increase in normal compression stress. The effect of the variation of the normal compression stress would be small.
- In the sequence of shaking table tests, dynamic responses including sliding and rocking became notable with increasing of the intensity of the inputs. The JMA Kobe 100% excitation, whose peak acceleration exceeded 0.8 g, exhibited maximum uplift and cumulative uplift of the two-story specimen approximately 15 times that of the 50% intensity shaking. A significant rock-slide response was noted under this shaking condition. The combination of the intensive acceleration input and significant rocking responses could result in the uplifted specimen sliding at this time, causing rock-slide behavior. The cumulative slide distance reached 381 mm; however, only a few cyclic slides occurred at the same locations along the moving track. Most surfaces sustained single slides. Similar results can be observed in other shaking conditions. The insufficient cyclic sliding and significant rocking resulted in a few graphite layers on the mortar surfaces. In addition, significant rocking caused impacts and stress concentration on the mortar surface when the uplifted base collided with the mortar and lead to surface crushes in several locations. The insufficient graphite lubrication and unsmooth surface condition might contribute to the variation of friction coefficient.
- Friction coefficients observed from shaking table tests were generally similar to those obtained in the preliminary friction tests; however, the values fluctuated more significantly under the JMA Kobe wave than did those for the specimen tested by the near fault ground motion, namely the TCU052 wave, especially for the 100% intensity excitations of the JMA Kobe wave. The maximum friction coefficient reached 0.8. JMA Kobe waves predominated at higher frequencies, and this might have been the main cause of their higher rocking response than those of TCU052 waves. The collisions due to rocking was found to cause strong vertical and horizontal acceleration impulses on the structure and resulted in the friction coefficient, which was the ratio of horizontal inertial forces to gravity, jumping to a high value under each collision.
- The strong horizontal acceleration responses caused by the collisions made the free-standing specimen unable to reduce the input horizontal acceleration notably, even when slippage occurred. Comparing with the fixed-base specimen whose roof horizontal response was amplified by approximately 1.8 times to reach 1.4 g under the JMA Kobe 100% shaking condition, the roof response of the free-standing specimen was amplified by approximately 1.4 times the input intensity. The

horizontal acceleration response amplification was reduced by approximately 20%. The first-story interstory drift in the free-standing specimen was approximately 0.25%, which declined to around 30% compared with that of the fixed-base specimen.

Acknowledgments

The authors would thank for the advice and support of professor George-C. Yeo, and the technical support of the technicians of NCREE South Lab.

References

Amiri, G.G., Shakouri, A., Veismoradi, S. and Namiranian, P. (2017), "Effect of seismic pounding on buildings isolated by triple friction pendulum bearing", *Earthq. Struct.*, **12**(1), 35-45. https://doi.org/10.12989/eas.2017.12.1.035.

Bakhshi, A., Araki, H. and Shimazu, T. (1998), "Evaluation of the performance of a suspension isolation system subjected to strong ground motion", *Earthq. Eng. Struct. Dyn.*, **27**(1), 29-47. https://doi.org/10.1002/(SICI)1096-9845(199801)27:1<29.

Campbell, W.E. (1939), "Studies in boundary lubrication", *Tran. ASME*, **61**, 633-641.

Chang, S., Makris, N., Whittaker, A.S. and Thompson, A.C.T. (2002), "Experimental and analytical studies on the performance of hybrid isolation systems", *Earthq. Eng. Struct. Dyn.*, **31**(2), 421-443. https://doi.org/10.1002/eqe.117.

Constantinou, M.C., Whittaker, A.S., Kalpakidis, Y., Fenz, D.M. and Warn, G.P. (2007), "Performance of seismic isolation hardware under service and seismic loading", Report No. MCEER-07-0012, Multidisciplinary Center for Earthquake Engineering Research, New York.

Editorial Committee for the Report on the Hanshin-Awaji Earthquake Disaster (1997), Report on the Hanshin-Awaji Earthquake Disaster, building series, Structural damage to steel buildings, Vol. 3, Architectural Institute of Japan, Tokyo, Japan. (in Japanese)

Enokida, R. and Nagae, T. (2017), "Seismic damage reduction of a structural system based on nontraditional sliding interfaces with graphite lubrication", *J. Earthq. Eng.*, **22**(4), 666-686. https://doi.org/10.1080/13632469.2016.1264326.

Fakhouri, M.Y. and Igarashi, A. (2013), "Multiple-slider surfaces bearing for seismic retrofitting of frame structures with soft first stories", *Earthq. Eng. Struct. Dyn.*, **42**(1), 145-161. https://doi.org/10.1002/eqe.2198.

Hsiao, C.P., Ding, Y.C., Sheu, M.S. and Tsai, K.C. (1999), "Investigation report of the 921 Chi-Chi earthquake: structural damages", Report No. NCREE-99-054, National Center for Research on Earthquake Engineering (NCREE). (in Chinese)

Japan Meteorological Agency, http://www.data/jma.go.jp/svd/eqev/data/kyoshin/jishin/hyogo_nanbu/index.html.

Kajiwara, K., Tosauchi, Y., Sato, E., Fukuyama, K., Inoue, T., Shiohara, H., Kabeyasawa, T., Nagae, T., Fukuyama, H., Kabeyasawa, T. and Mukai, T. (2017), "Three-dimensional shaking table test of a 10-story reinforced concrete building on the E-defense Part 1: Overview and specimen design of the base slip and base fixed tests", *16th World Conference on Earthquake Engineering*, Santiago, Chile, January.

McCormick, J., Nagae, T., Ikenaga, M., Zhang, P., Katsuo, M. and Nakashima, M. (2009), "Investigation of the sliding behavior between steel and mortar for seismic applications in structures", *Earthq. Eng. Struct. Dyn.*, **38**(12), 1401-1419. https://doi.org/10.1002/eqe.908.

Mokha, A., Constantinou, M., Reinhorn, A. and Zayasm V. (1991), "Experimental study of friction-pendulum isolation system", *J. Struct. Eng.*, **117**(4), 1201-1217. https://doi.org/10.1061/(ASCE)0733-9445(1991)117:4(1201).

Mokha, A., Constantinou, M.C. and Reinhorn, A.M. (1990), "Teflon bearings in base isolation. I: Testing", *J. Struct. Eng.*, **116**(2), 438-454. https://doi.org/10.1061/(ASCE)0733-9445(1990)116:2(438).

Mostaghel, N. and Khodaverdian, M. (1987), "Dynamics of resilient-friction base isolator (R-FBI)", *Earthq. Eng. Struct. Dyn.*, **15**(3), 379-390. https://doi.org/10.1002/eqe.4290150307.

National Center for Research on Earthquake Engineering, (NCREE), https://www.ncree.org/Ncree.aspx?id=4.

Rabbat, B. and Russel, H. (1985), "Friction coefficient of steel on concrete or grout", *J. Struct. Eng.*, **111**(3), 505-515. https://doi.org/10.1061/(ASCE)0733-9445(1985)111:3(505).

Sato, E., Tosauchi, Y., Fukuyama, K., Inoue, T., Kajiwara, K., Shiohara, H., Kabeyasawa, T., Nagae, T., Fukuyama, H., Kabeyasawa, T. and Mukai, T. (2017), "Three-dimensional shaking table test of a 10-story reinforced concrete building on the E-defense Part 2: Specimen fabrication and construction, test procedure, and instrumentation program", *16th World Conference on Earthquake Engineering*, Santiago, Chile, January.

Tassios, T. and Vintzeleou, E. (1986), "Concrete-to-concrete friction", *J. Struct. Eng.*, **113**(4), 832-849. https://doi.org/10.1061/(ASCE)0733-9445(1987)113:4(832).

Tiong, P.L.Y., Adnan, A., Rahman A.B.A. and Mirasa, A.K. (2014), "Seismic base isolation of precast wall system using high damping rubber bearing", *Earthq. Struct.*, **7**(6), 1141-1169. https://doi.org/10.12989/eas.2014.7.6.1141.

Tosauchi, Y., Sato, E., Fukuyama, K., Inoue, T., Kajiwara, K., Shiohara, H., Kabeyasawa, T., Nagae, T., Fukuyama, H., Kabeyasawa, T. and Mukai, T. (2017), "Three-dimensional shaking table test of a 10-story reinforced concrete building on the E-defense Part 3: Base slip and vase fixed test results", *16th World Conference on Earthquake Engineering*, Santiago, Chile, January.

Tsai, K.C., Hsiao, C.P. and Bruneau, M. (2000), "Overview of building damages in 921 Chi-Chi Earthquake", *Earthq. Eng. Eng. Seismol.*, **2**(1), 93-108.

Tsopelas, P., Constatinou, M.C., Kim, Y.S. and Okamoto, S. (1996), "Experimental study of FPS system bridge seismic isolation", *Earthq. Eng. Struct. Dyn.*, **25**(1), 65-78. https://doi.org/10.1002/(SICI)1096-9845(199601)25:1<65.

Zayas, V.A., Low, S.S. and Mahin, S.A. (1990), "A simple pendulum technique for achieving seismic isolation", *Earthq. Spectra*, **6**(2), 317-333. https://doi.org/10.1193/1.1585573.

KT